Rotation and sliding collapse mechanisms for in plane masonry pointed arches: statistical parametric assessment

Alejandro Jiménez Rios[a,*], Bledian Nela[a], Marco Pingaro[a], Emanuele Reccia[b], Patrizia Trovalusci[a]

[a] *Dept. of Structural and Geotechnical Engineering., Sapienza University of Rome, Via Gramsci 53, 00197, Rome, Italy.*
[b] *Dept. of Civil and Environmental Engineering and Architecture, University of Cagliari, Via Marengo 2, 09123, Cagliari, Italy.*

Abstract

Pointed arches are important architectural elements of both western and eastern historical built heritage. In this paper, the effects that different geometrical (slenderness and sharpness) and mechanical (friction and cohesion) parameters have on the in-plane structural response of masonry pointed arches are investigated. Two load scenarios are studied: vertical self-weight plus a proportional horizontal live load and vertical self-weight plus a vertical concentrated live load applied to individual voussoir. Results, in terms of collapse multipliers and collapse mechanisms, are presented and analysed following a systematic statistical approach.

Keywords: `Non-standard Limit Analysis`, `Friction/Dilatancy`, `No-tension contacts`, `Pointed arches`, `Cohesion`

1. Introduction

Pointed arches are well known as representative elements of the Gothic style in western architecture. However, according to certain authors, pointed arches first appeared in Persian architecture, during the Sassanid Empire (third to seventh century AD) and then were adopted by muslim architecture at the begining of the eighth century. According to Viollet-le-duc, pointed arches were found both in Persia and Egypt

*Corresponding author: alejandro.jimenezrios@uniroma1.it

as early as the sixth century and this architectural element was not introduced in Europe until the twelfth century [1]. Figure 1 presents an example of pointed arches used in western architecture (Figure 1a) and in muslim architecture (Figure 1b).

(a) (b)

Figure 1: Examples of pointed arches in: (a) western architecture, Brussels cathedral windows, Belgium and (b) muslim architecture, El Badi palace at Marrakech, Morocco.

Despite the fact that it has been well known for a long time that pointed arches have a different structural behaviour in comparison to circular arches, i.e. classic geometric rules prescribed thinner abutments for pointed arches than for circular arches [1], relatively little attention has been paid to the formal structural study of the former. Aita *et. al* [2] studied the equilibrium of circular, pointed and elliptical arches subjected to their own self-weight plus the superimposed weight of a masonry wall. They applied the Durand-Claye's method and a nonlinear one-dimensional elastic analysis and found that pointed and elliptical arches had a better behavior in comparison to circular ones in terms of wall height that can be carried by the arch. Cavalagli *et. al* [3] and Brandonisio *et. al* [4] consider the effect of the uncertain dimension of the blocks and the effect of the buttresses on the seismic capacity of arches, respectively. Misseri and Rovero [5] adopted the Heyman's hypothesis and analysed the seismic vulnerability of pointed arches through a parametric analysis that explored arch slenderness and sharpness. Based on their results, it is now known that the pattern of hinges at collapse for pointed arches differs considerably from the one of circular arches, that a slenderness*sharpness interaction effect is significant on collapse accelerations and that the acceleration to start motion is directly proportional to arch rise in pointed arches, contrary to the case of circular ones. Also by adopting Heyman's hypothesis, Cavalagli

et. al [6] studied the limit equilibrium condition and the minimum thickness of circular and pointed masonry arches subjected to vertical self-weight plus a horizontal proportional live load. They provided a series of surface plots from which the collapse multiplier of either type of arch could be determined based on their geometry parameter values. Misseri *et. al* [7] performed an experimental campaign in which they studied the response of pointed arches subjected to vertical self-weight and a proportional horizontal live load for different values of slenderness and sharpness by means of a tilting table. They identified two types of collapse mechanism: pure rotation and rotation/sliding combination (their experimental set-up prevented the formation of pure sliding collapse mechanisms). Moreover, a significant effect on the response caused by the sharpness*slenderness parameter combination was observed, in other words, load multipliers recorded for the thicker profiles increase slower than thinner profiles. In a recent application of Durand-Claye's method, Aita *et. al* [8] presented the characteristic mechanical behaviour and collapse of symetric circular, low-pointed, equilateral-pointed and lancet-pointed arches subjected to self-weight for which friction coefficient and compressive strength was taken into account. Later on they extended their work to the analysis of the same arches typologies supported on piers [9]. Recently, Misseri *et. al* [10] studied the vulnerability of masonry pointed arches subjected to support displacements through a novel numerical approach that uses combinatorial laws and adopts Heyman's assumptions. According to the observations made by Romano and Ochsendorf [11] it could be said from the structural behaviour of pointed arches that:

- Pointed arches have lower horizontal thrust than circular arches.
- Under symmetrical conditions, the thrust line of a circular arch touches the extrados at only one location, whereas that on a pointed arch, due to its geometry, the thrust line has to touch the extrados twice and for extremely thin pointed arches it touches twice the extrados and once the intrados.
- Pointed arches for most practical geometries can be thinner than their circular counterparts with few uncommon exceptions for arches with low embrace angles.

- Pointed arches subjected to horizontal support spreading are able to deform substantially more than circular ones.
- Pointed arches can support higher concentrated loads at the crown than circular ones.

Due to masonry heterogeneity and to effect of geometrical parameters have on its behaviour, the simulation of masonry structural response and assessment is a complicated task. Over the past decades a variety of numerical approaches have been proposed by several authors trying to reproduce masonry structural behaviour at different scales and levels of detail. Among the more suitable strategies to capture masonry structural response are the so called block-based models (BBM). They are discrete models in which every masonry block is modelled along with a suitable formulation to represent the inter-block interactions. In this context, Limit Analysis permits the evaluation of the ultimate load capacity of the structure and its corresponding failure mechanism, requiring a limited number of material parameters, overcoming the common difficulties of obtaining reliable experimental data for historical masonry structures. Furthermore, Limit Analysis is largely recognized as a very effective tool to estimate collapse load and collapse mechanisms for masonry structures [12, 13, 14, 15, 16, 17, 18, 19] or masonry structures in presence of settlements [20, 21, 22].

Starting from the work of [13], a new version of the *ALMA* code (Analisi Limite Murature Attritive) has been developed based on the Limit Analysis [23, 24, 25] namely *ALMA 2.0*. The new version of *ALMA* by the adoption of the recent coding language *Python*^{TM} and the advantages of the novel optimization subroutine, such as *MOSEK* library (www.mosek.com), overcomes the limit in terms of number of blocks with respect to the original version [13] and it has been improved in order to take into account foundation settlement [21], cohesion between the joints and retrofitting tie [23]. The capabilities of *ALMA 2.0* to reproduce the structural response of in-plane masonry pointed arches has already been validated [26] using as benchmark the experimental results and numerical simulations performed by Misseri *et al.* [7].

In this paper the effect of different geometrical and mechanical parameters in the in-plane structural response of masonry pointed arches using a non-standard analysis

approach is presented. In particular the adopted approach is based on the one provided in [12, 13], in which authors demonstrated that a non associative problem with friction can be approximated by a standard, associative, approach where friction has been replaced by dilatancy. In this way, the peculiar effect of the sliding mechanism, which can occur also in the arches with high value of thickness, may be taken into account in the analysis performed.

The main difference of this work with respect to parametric analysis performed by other authors, is the fact that a systematic statistical approach has been implemented which has enabled the authors not only to identify, but also to quantify, the effect on the response of the different factors studied. First the formulation of the non-standard limit analysis implemented is described in Section 2, followed by the description of the systematic parametric analysis used in Section 3. Then, the results obtained in terms of collapse multipliers and collapse mechanisms are shown and discussed in Section 4. Finally, in Section 5, the main conclusions drawn from the analysis and discussion of the results are summarized.

2. Adopted Model

We consider Limit Analysis of systems of rigid blocks interacting through non-tension and frictional interfaces. In this case the normality rule does not hold and the problem is non-associative and can be solved using non-linear programming procedures [12, 13]. It is known differently, that, when normality rule holds the static and kinematic theorems of Limit Analysis lead to two dual problems of linear programming, with a unique solution. We decided to focus on the linear programming optimization problem (firstly developed in the seminal paper by [27] following a lower bound approach). In particular, to overcome problem related to the solution of the non associative problem we refer to the approach in [13], where friction is replaced by dilatancy obtaining a linearized programming problem, which provides collapse mechanisms and collapse load of analysed structures.

Following this idea, linear programming has been performed taking into account both rotation and sliding mechanisms at the interfaces between blocks. The adopted

kinematic upper bound problem is defined as:

$$\alpha_c = \min \left\{ \boldsymbol{\lambda}^T \left[\boldsymbol{c} - \left(\boldsymbol{A}_0 \boldsymbol{N}_1 \right)^T \boldsymbol{f}_0 \right] \right\} \tag{1}$$

subjected to:

$$\left(\boldsymbol{A}\boldsymbol{N}_1 - \boldsymbol{N}_2 \right) \boldsymbol{\lambda} = \boldsymbol{0} \,, \text{ compatibility condition}$$

$$\boldsymbol{\lambda}^T \left(\boldsymbol{A}_0 \boldsymbol{N}_1 \right)^T \boldsymbol{f}_L - 1 = 0 \,, \text{ normalized positive work of live loads}$$

$$\boldsymbol{\lambda} \geq \boldsymbol{0} \text{ bounds on the unknowns.}$$

In the above equations the unknown of the problem remains α_c, a scalar, as the collapse multiplier with $\boldsymbol{\lambda}$ as the plastic multiplier vector that contains the nonnegative coefficients. $\boldsymbol{A}_0$ is the inverse matrix of the compatibility kinematical submatrix of maximum rank while the rest of the kinematical matrix $\boldsymbol{B}_2$ is stored in the $\boldsymbol{A}$ matrix as $\boldsymbol{A} = \boldsymbol{B}_2 \boldsymbol{B}_1^{-1}$. $\boldsymbol{N}_1$ and $\boldsymbol{N}_2$ are the submatrices of the block-diagonal gradient matrix $\boldsymbol{N}$ and correspond to the submatrix of independent and linearly dependent kinematical variables, respectively. $\boldsymbol{f}_0$ and $\boldsymbol{f}_L$ are the vectors of the generalized actions on the centres of the blocks for the dead and live loads, respectively. Additional details on the derivations and formulation of the LP problem can be consulted in [28, 12]. Different cohesion values can be assigned to every joint of the masonry assemblage. These values are stored in the form of a vector $\boldsymbol{c}$. A Mohr-Coulomb classical yield domain is considered with the inclusion of cohesion, thus indirectly involving tensile strength of the joints as $\boldsymbol{\sigma}_t = \boldsymbol{c} / \tan \phi$, for $\boldsymbol{\sigma}_t$ as the tensile strength and ϕ as the friction angle. After some algebraic operations the $\boldsymbol{c}$ vector is stored in the objective function to be minimized through LP.

3. Design of experiments (DOE)

A systematic methodology has been followed in order to objectively determine the influence of several mechanical and geometrical parameters in the response of pointed arches. Thus, general full factorial designs were used to identify both the main and the two-way interaction effects of the studied parameters on the pointed arches response. Two load scenarios were considered, the first one in which the pointed arches were

subjected to their own self-weight plus a horizontal live load proportional to the self-weight, henceforth referred as scenario A, and a second load scenario in which the pointed arches were subjected to their own self-weight plus a vertical concentrated live load applied to one of their voussoirs proportional to its self-weight, from now on referred as scenario B. The factors considered for each scenario and their correspondent levels (in this context, a level refers to a particular value adopted by a parameter or factor) are presented in Table 1.

Table 1: Studied factors and their respective levels for a pointed arch subjected to load scenario A and B.

	Scenario A			**Scenario B**	
Factor	**Level**	**Value**	**Factor**	**Level**	**Value**
A. Cohesion (MPa)	1. Low	0.00	A. Cohesion (MPa)	1. Low	0.00
	2. Medium	0.01		2. Medium	0.01
	3. High	0.10		3. High	0.10
B. Friction (-)	1. Lowest	0.47	B. Friction (-)	1. Lowest	0.47
	2. Low	0.60		2. Low	0.60
	3. High	0.84		3. High	0.84
	4. Highest	1.00		4. Highest	1.00
C. Sharpness (-)	1. Low	0.20	C. Slenderness (-)	1. Lowest	0.10
	2. Medium	0.60		2. Low	0.15
	3. High	1.00		3. High	0.20
				4. Highest	0.25
D. Slenderness (-)	1. Lowest	0.10	D. Live load (-)	1. Lowest	8
	2. Low	0.15		2. Low	10
	3. High	0.20		3. High	12
	4. Highest	0.25		4. Highest	14

Mathematically speaking the values that could be adopted for the friction angle ϕ (in degrees) could lay within the interval $0 < \phi < 90$. Moreover, masonry friction angles have been experimentally determined by several researchers in the past and the values reported oscillate between the 17 and the 63 degrees [29]. However, most commonly friction angle values for historical masonry vary between 15 and 45 degrees

and more specifically for arches between 25 and 45 degrees. Therefore, the different levels for friction, $tan\phi$, studied were 0.47, 0.60, 0.84 and 1.00 which correspond to 25, 30, 40 and 45 degrees respectively. The low friction values adopted would represent a situation in which the units surface were relatively smooth, whereas that a rough surface would be better represented by the high friction values assumed.

The geometrical parameters, sharpness and slenderness, are better understood having as reference Figure 2. In this figure, the center of the arch is indicated by O. The arch has a diameter R_p and it is drawn with two circles that have their corresponding center points at points C_1 and C_2 which are located at an eccentricity distance e from the arch center O. t indicates the thickness of the arch and R_i and R_e represent the internal and the external radius of the arch measured from the corresponding excentric centers C_1 and C_2. Finally, R_c is the distance from O to the center of the arch at its base.

Slenderness is defined as the ratio between the thickness of the arch and its radius, $S_d = t/R_c$. Sharpness is equal to the division of the arch excentricity by the distance from O to the center of the arch at its base, $S_h = e/R_c$. The numerical values for Slenderness and Sharpness adopted in this work correspond with those experimentally reported by [7] and numerically validated by [26]. Therefore, the combination of three sharpness values and four slenderness values resulted in the twelve arches shown in Figure 3.

The live load location parameter makes reference to the voussoir to which the concentrated live load is applied (see the values of the live load factor in Table 1). All pointed arches modeled in this study have been formed by 17 blocks, 16 voussoirs and a key block. The numbers assigned to each block are shown in Figure 4.

To the extend of the knowledge of the authors of this paper, there are not cohesion values reported in the literature for the specific case of pointed arches. In a comparative experimental work, Jafari *et al.* [30] reported a series of cohesion values obtained through testing of different masonry typology cores and triplets. The cohesion values obtained from the shear tests on cores ranged from 0.13 up to 0.49 MPa, whereas that the values obtained from the triplets ranged from 0.08 up to 0.54 MPa. Through the implementation of a static penetrometer, Liberatore *et al.* [31] determined the cohe-

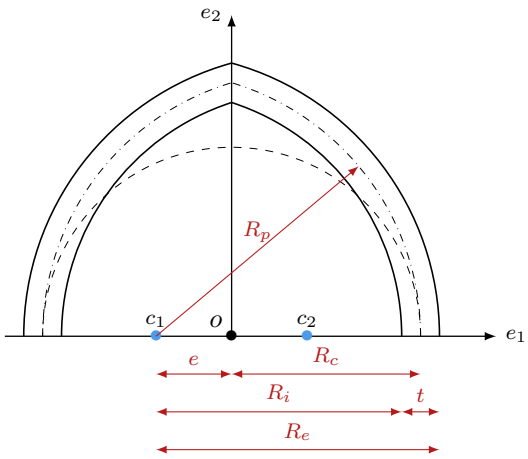

Figure 2: Schematic geometry of the pointed arches simulated.

sion values of several decayed historical masonry walls mortar. The cohesion values reported by these authors ranged from 0.02 up to 0.03 MPa. On Bejarano-Urrego *et al.* [32] a table with values for different masonry joints properties is presented. The values for cohesion, based on the information reported by several authors, vary from 0.1 to 1.8 MPa. By testing a series of triplets created with different masonry units and mortar, Milosevic *et al.* [33] determined cohesion values in the range of 0.2 - 1.6 MPa. These authors also tested a series of stone masonry wallettes through the diagonal compression test for which they obtained cohesion values in the range of 0.017 and 0.313 MPa. Furthermore, they compared the values they obtained through their experimental campaign with the ones reported in the literature which ranged between the 0.02 and the 0.16 MPa.

The cohesion values that are adopted to perform numerical analysis depend significantly in the numerial approach followed. Rafiee and Vinches [34] simulated the structural response of stone masonry arches with the use of a non-smooth contact dynamics method. For their simulations, these authors adopted for their models cohesion values of 0.010 and 0.007 for the normal and tangential cohesion thresholds parameters respectively. Masi *et al.* [35] adopted cohesion values ranging from 0.0 to 3.0 MPa to perform a sensitivity analysis of arched masonry structures under blast loads using

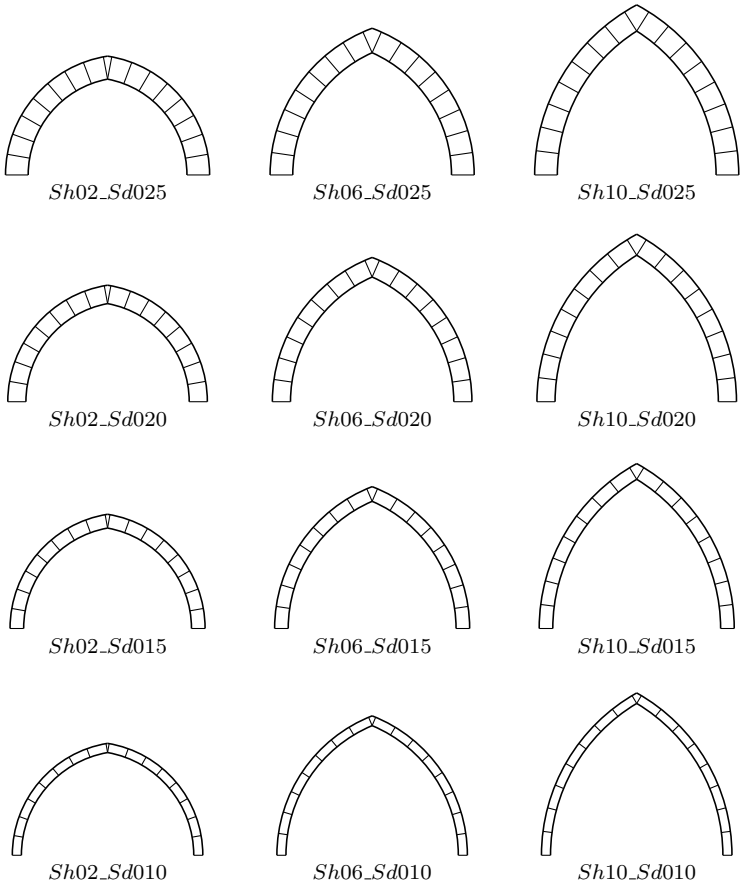

Figure 3: Geometries of the simulated arches.

a discrete element method based-approach. Weed *et al.* [36] adopted cohesion values of 0.67 and 0.116 MPa to simulate the interface cohesion of cement stabilized soil block masonry walls subjected to four-point out-of-plane bending using a finite element method based-approach. On recent numerical calibrations of irregular stone masonry walls, Zhang and Beyer [37] implemented a cohesion value of 0.3 MPa to describe the properties of their finite element model. In this work, a null cohesion value has been adopted to simulate the structural response of dry stone masonry pointed arches. Moreover, relatively low values of cohesion (0.01 and 0.10 MPa) have been adopted to better represent the condition of historical stone masonry pointed arches with decayed

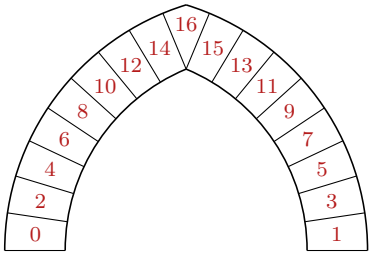

Figure 4: Numbers assigned to every block of the modeled pointed arches.

or damaged mortar.

Other important simulation parameters adopted in this work correspond to the thickness of the blocks, which was assumed to be fixed for all arches at a value of 50 mm as well as a constant specific weight of 1800 kg/m^3. As this was a numerical experiment, the basic principles of randomization, replication and blocking resulted trivial (as these were numerical simulations, regardless of the order in which they are run, the number of times they are run or the way in which they are grouped, the answer obtained is always the same. This is usually not the case when real life experiments are performed since the response may be affected by non-controlled factors).

After all simulations were successfully run, the responses (collapse multipliers) obtained were visually analysed by the means of main effects and two-way interaction effects plots. The main effect plots enable the observation of the actual effect that every single parameter has in the response. By computing the mean values at every level of each parameter it is assumed that the response is independent of the other parameters. On the other hand, two-way (or higher order) interaction plots allow to study the possible interaction between two or more parameters and how this affects the response. The points of a two-way interaction plot are computed by averaging the values of α_c obtained for a certain combination of two parameters' levels.

Furthermore, the collapse multipliers obtained were formally analysed through an analysis of variance (ANOVA). The ANOVA, sometimes referred to as significance of regression test, determines whether there is a relationship between the parameters of the statistical model (also known as regressor variables) and the response. The hypotheses

of the ANOVA test are:

$$\begin{aligned} &H_0 : \beta_1 = \beta_2 = ...\beta_k = 0 \ , \\ &H_1 : \beta_j \neq 0 \text{ for at least one } j \ . \end{aligned} \tag{2}$$

Where H_0 and H_1 are the null and the alternative hypothesis respectively, and β_j represents every linear and two-way interaction term of the statistical model adopted. The rejection of H_0 implies that at least one of the terms contributes significantly to the statistical model. The statistical model adopted for the pointed arches under load scenario A is composed by four linear terms (cohesion, friction ratio, sharpness and slenderness), six two-way interaction terms (combinations of the four linear terms previously mentioned) and an error term. Similarly, the statistical model for the load scenario B is composed by four linear terms (cohesion, friction ratio, slenderness and live load location), six two-way interaction terms and an error term. Linear terms correspond to the effect that individual parameters have in the response whereas that two-way interaction terms depict how the response is affected by a certain parameter in combination with the different levels of a second one. The error term is related to the inherent variation of the model and is assumed to be normally and independently distributed.

Additionally, the magnitude and importance of each one of the main factors and factor interaction effects were obtained. Those results are presented as Pareto charts of standardized effect. The Pareto chart of standardized effects is used to compare the relative magnitude and the statistical significance of the main parameters and of the two-way interaction terms in the response. Moreover, a reference line is also plotted in the Pareto chart in order to simplify the identification of the significant terms (every term with a standardized effect value higher than the reference line is considered to be statistically significant).

The suitability of the adopted statistical models to describe the response, was measured as the values of the coefficient of determination, R^2 (equal to the regression sum of squares divided by the total sum of squares), and of the predicted coefficient of determination, R^2_{pred}. Finally, the assumptions that the data was independent and normally

distributed, in other words, that the analysed data was not affected by non-controlled parameters and that it roughly presents the shape of the Gauss curve, were visually validated by analysing the standardized residual plots of the response, α_c, its histogram and its normal probability plot.

4. Results and discussion

4.1. Collapse mechanisms

4.1.1. Collapse mechanisms under load scenario A

Regarding the collapse mechanisms of the pointed arches under load scenario A and for the specific case of null cohesion (dry stone masonry), it could be said that three different outcomes were observed: pure rotation, pure sliding and rotation-sliding collapse modes. The pure rotation collapse mode appeared mainly on slender pointed arches and in medium-slender pointed arches with high friction ratio values such as the example arches shown in Figure 5. The pure sliding collapse mode only developed for the pointed arch with a sharpness value of 0.10, a slender value of 0.25 and a friction ratio of 0.47 (see Figure 6). Finally, the combination of rotation/sliding collapse mode was the most common one developed by the pointed arches studied as can be seen in the arches of Figure 7.

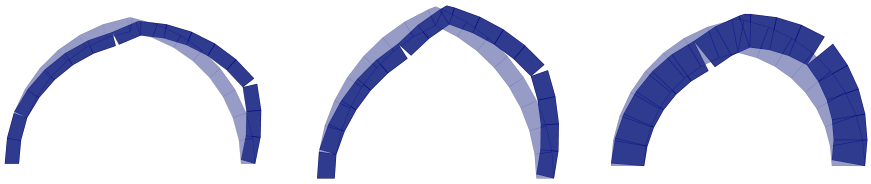

(a) Friction 0.47, Slenderness 0.10, Sharpness 0.20 and $\alpha_c = 0.08529$.

(b) Friction 0.84, Slenderness 0.10, Sharpness 0.60 and $\alpha_c = 0.16921$.

(c) Friction 1.00, Slenderness 0.25, Sharpness 0.20 and $\alpha_c = 0.46179$.

Figure 5: Rotation collapse mechanisms of dry masonry (null cohesion values) slender pointed arches or with relatively high friction values under load scenario A.

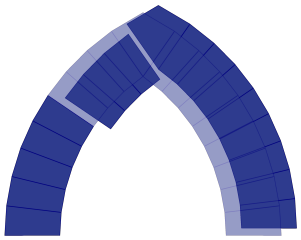

Figure 6: Sliding collapse mechanisms of pointed arch with Friction 0.47, null cohesion, Slenderness 0.25 and Sharpness 1.00 under load scenario A, $\alpha_c = 0.30370$.

The collapse mechanisms observed for the no-cohesion cases were clearly modified by the inclusion of cohesion. For cohesion values of 0.01 MPa only pure rotation and rotation-sliding mechanisms developed, whereas that only rotation mechanisms were obtained for the pointed arches with a cohesion value of 0.10 MPa. The most clear example of the role that cohesion plays in the collapse mechanism of the pointed arches studied can be observed for an arch with a slenderness value of 0.10 and a sharpness value of 0.25. Figure 8 presents the collapse mechanisms obtained for this arch for cohesion values of 0.00 MPa (a), 0.01 MPa (b) and 0.10 MPa (c) (and a friction ratio value of 0.47). The collapse mechanism obtained for the dry stone masonry arch (no-cohesion) was of pure sliding, the one for the arch with an intermediate cohesion value (0.01 MPa) was of the combined rotation-sliding type whereas that a pure rotation collapse mechanism was obtained for the arch with a relatively high cohesion value (0.10 MPa).

4.1.2. Collapse mechanisms under load scenario B

The effect that cohesion, friction ratio and slenderness have in the collapse mechanism of pointed arches has already been discussed in a previous section for the case of pointed arches under load scenario B. Similar observation could be made about these parameters for the case of pointed arches under load scenario B. On the other hand, the effect that the location of the live load has in the response of pointed arches is

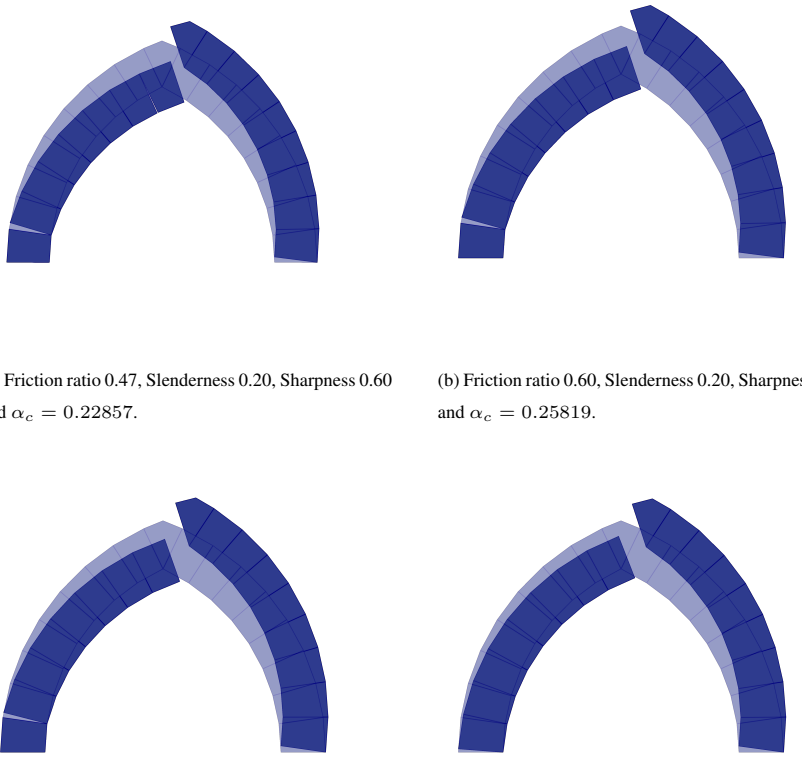

(a) Friction ratio 0.47, Slenderness 0.20, Sharpness 0.60 and $\alpha_c = 0.22857$.

(b) Friction ratio 0.60, Slenderness 0.20, Sharpness 0.60 and $\alpha_c = 0.25819$.

(c) Friction ratio 0.84, Slenderness 0.20, Sharpness 0.60 and $\alpha_c = 0.31495$.

(d) Friction ratio 1.00, Slenderness 0.20, Sharpness 0.60 and $\alpha = 0.34739$.

Figure 7: Combined collapse mechanisms for dry masonry pointed arches under load scenario A.

presented now. The collapse mechanisms obtained for pointed arches with a medium value of cohesion (0.01 MPa), a low slenderness value (0.15), a low friction ratio (0.60) and the live load applied at blocks 8, 10, 12 and 14 is presented in Figure 9 (a), (b), (c) and (d) respectively. As it can be observed, the effect of placing the live load in either blocks 8 or 10 will lead to a pure rotation mechanism, whereas that if the live load is applied in either blocks 12 or 14, the collapse mechanism generated is of the combined rotation-sliding type.

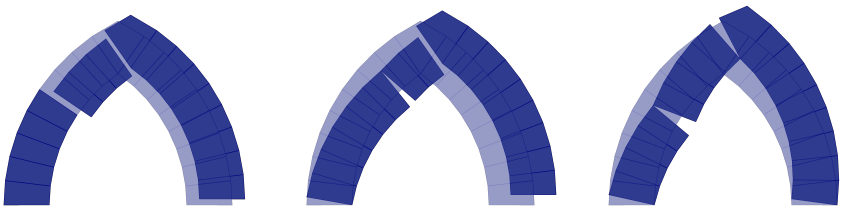

(a) Friction ratio 0.47, Slenderness 0.25, Sharpness 1.00, cohesion 0.00 MPa and $\alpha_c = 0.30370$.

(b) Friction ratio 0.47, Slenderness 0.25, Sharpness 1.00, cohesion 0.01MPa and $\alpha_c = 0.61368$.

(c) Friction ratio 0.47, Slenderness 0.25, Sharpness 1.00, cohesion 0.10 MPa and $\alpha_c = 2.71721$.

Figure 8: Effects of cohesion in the collapse mechanisms of pointed arches under load scenario A.

4.2. Collapse multipliers

4.2.1. Collapse multipliers under load scenario A

After running the limit analysis numerical simulations of all the pointed arches subjected to their own self weight plus a horizontal live load proportional to their self-weight (load scenario A) as described in Section 3, the corresponding collapse multipliers were obtained. These values were used to determine if any of the analyzed parameters had a statistically significant influence in the response. To do so, the mean value of α_c was computed at every level for all individual factors and combination of two factors. The main effect plots are shown in Figure 10 and the two-way interaction plots are presented in Figure 11.

From Figure 10 it can be observed that all factors present a positive relation with the response (the higher is the value of the factor, the higher is the collapse multiplier obtained). Both friction ratio and sharpness have a relatively weak effect on the response whereas that cohesion and slenderness present a strong relation.

From the first row of the curves shown in Figure 11 it can be observed that there is no statistically significant interaction between cohesion*friction interactions, as the average α_c values at the different levels of the combined parameters are practically identical as well as the variability of results obtained at the different levels combinations. Although the slenderness-sharpness curves (observed in the lower right part of

Figure 11) present higher values of average collapse multipliers for higher values of slenderness, it can be observed that the variability of the response is quite identical at the three levels of sharpness, thus showing that this two-way interaction term does not cause significant effects on the response. On the other hand, a clear two-way interaction effect is detected for the two-way parameter interaction of cohesion-slenderness. At a null cohesion value (dry stone masonry) the response varies slightly for the different levels of slenderness. As the cohesion value increases, so does the variability of the response for the higher values of slenderness, a significantly higher collapse multiplier is obtained in comparison with the lower values of slenderness. There is a similar effect in the response caused by the two-way parameter interactions of friction*slenderness, friction*sharpness and cohesion*sharpness. Although the variability of the response (relatively higher collapse multipliers for the higher values of the mentioned parameters combinations) is not as vissually obvious as for the cohesion*slenderness combination, it could be considered that these three two-way terms affect the response in a significant way as well.

To verify the assumptions adopted after the visual examination of Figures 10 and 11, the collapse multipliers obtained were analysed through an analysis of variance (ANOVA). Table 2 presents the ANOVA results performed using the software *Minitab*® (`https://www.minitab.com/en-us/`). In the first column of Table 2 the statistical model terms are identified by their names, in the second column the degrees of freedom (DoF) of every term are presented, in the third column the adjusted sum of squares (Adj SS) corresponding to every term are shown and in column four the adjusted mean squares (Adj MS) are listed. In the fifth column of the ANOVA table we can see the value corresponding to the F statistical test and finally, in the last column of Table 2, the corresponding P-Values to each term are presented. At a confidence level of 95%, the terms with a $P - Value < 0.05$ are considered to be statistically significant. Thus, besides from the cohesion*friction and the sharpness*slenderness two-way interaction terms, the rest of the terms in the statistic model adopted are considered to have a significant effect in the response of the pointed arches studied.

Moreover, the magnitude and importance of each one of the main factors and factor interaction effects were obtained. In Figure 12 it can be seen that besides from

Table 2: ANOVA table of the pointed arches under load scenario A.

Source	**DoF**	**Adj SS**	**Adj MS**	**F-Value**	**P-Value**
Model	47	104.754	2.2288	979.62	0.000
Linear	10	96.165	9.6165	4226.73	0.000
Cohesion	2	83.457	41.7287	18340.95	0.000
Friction	3	0.182	0.0607	26.66	0.000
Sharpness	2	0.186	0.0929	40.85	0.000
Slenderness	3	12.340	4.1133	1807.91	0.000
Two-Way Interactions	37	8.588	0.2321	102.02	0.000
Cohesion*Friction	6	0.024	0.0040	1.76	0.115
Cohesion*Sharpness	4	0.115	0.0289	12.68	0.000
Cohesion*Slenderness	6	8.238	1.3729	603.45	0.000
Friction*Sharpness	6	0.133	0.0222	9.76	0.000
Friction*Slenderness	9	0.061	0.0068	2.98	0.004
Sharpness*Slenderness	6	0.017	0.0028	1.24	0.295
Error	96	0.218	0.0023		
Total	143	104.972			

DoF=Degrees of freedom, Adj SS= Adjusted sum of squares, Adj MS = Adjusted mean of squares.

the cohesion*friction and the sharpness*slenderness, all other terms on the statistical model resulted to have a significant effect in the response (as they all have a standardized effect value greater than the significance threshold of 1.985). All single parameter terms along with the two-way cohesion*slenderness interaction term were the terms of the model with a higher influence in the collapse multiplier value of the simulated values. These terms are followed in order of importance by the friction*sharpness and cohesion*sharpness terms, and finally by the friction*slendernes two-way interaction effect.

Regarding the suitability of the adopted statistical model to describe the response, the values of the coefficient of determination, R^2 and of the predicted coefficient of determination, R^2_{pred}, obtained were of 99.79% and 99.53% respectively. This proves

the good fit and the high prediction capabilities of the model adopted and allows to maintain the cohesion term of the statistical model as linear.

The data independence and data normality assumptions were visually validated by analyzing the standardized residual plots of the response, α_c, its histogram and its normal probability plot. In the normal probability plot of Figure 13 (upper right plot) it could be observed that most of the points were relatively close to the diagonal line and only a few outliers were present (one observation with a standardized residual value smaller than three and three observation with a value greater than three), which did not affect significantly the validity of the statistical model adopted. Furthermore, it could be observed that the histogram on Figure 13 resembles to a Gauss distribution and that no clear structure is present on the Versus Fits nor on the Versus order plots of the standardized residuals in Figure 13.

4.2.2. Collapse multipliers under load scenario B

As per the pointed arches subjected to a load scenario A, similar data was obtained and analyzed per the pointed arches under load scenario B. The main effect plots are shown in Figure 14 and the two-way interaction plots are presented in Figure 15. Table 2 presents the ANOVA results and Figure 16 the Pareto chart of standardized effects.

From Figure 14 it can be observed that both cohesion and slenderness have a strong positive relationship with the response, namely the higher the cohesion or the slenderness, the higher would be the value of α_c. The friction ratio parameter presents a relatively weak positive relation with the response. Finally, the live load location parameter plays an important role in the collapse multiplier value obtained from the pointed arches simulated under load scenario B. It can be observed that the closer the live load is applied to the key stone (see Figure 4), the lower will be the collapse multiplier obtained. From the curves of Figure 14 it can be seen that there is a non-linear relation between slenderness and live load location with the response of the pointed arch under load scenario B. Unfortunately, the terms for the individual parameters in the statistical model adopted are linear and this has cause some low values for the suitability, $R^2 = 83.57\%$, and the prediction, $R^2_{pred} = 66.77\%$, capabilities of the adopted

Table 3: ANOVA table of the pointed arches under load scenario B.

Source	**DoF**	**Adj SS**	**Adj MS**	**F-Value**	**P-Value**
Model	56	7609438	135883	12.26	0.000
Linear	11	3825111	347737	31.38	0.000
Cohesion	2	1282242	641121	57.86	0.000
Friction	3	27056	9019	0.81	0.488
Slenderness	3	1297822	432607	39.04	0.000
Live load	3	1217991	405997	36.64	0.000
Two-Way Interactions	45	3784327	84096	7.59	0.000
Cohesion*Friction	6	5094	849	0.08	0.998
Cohesion*Slenderness	6	890816	148469	13.40	0.000
Cohesion*Live load	6	753611	125602	11.34	0.000
Friction*Slenderness	9	47035	5226	0.47	0.892
Friction*Live load	9	33687	3743	0.34	0.961
Slenderness*Live load	9	2054084	228232	20.60	0.000
Error	135	1495795	11080		
Total	191	9105233			

DoF=Degrees of freedom, Adj SS= Adjusted sum of squares, Adj MS = Adjusted mean of squares.

statistical model. The statistical model could be further improved through a parameter transformation (adopting quadratic or exponential terms for the mentioned parameters) but that is outside the scope of this paper.

From the two-way interaction curves of Figure 15 it can be observed that cohesion*slenderness, cohesion*live load and slenderness*live load parameter interactions have a statistically significant effect of the response of pointed arches under load scenario B. The values obtained for the response changes significantly for the different parameter combinations mentioned (similar $< \alpha >$ values for the lower values of cohesion and slenderness regardless of the value of the second parameter, whereas relatively significant variation on the $\langle \alpha_c \rangle$ values for the higher values of cohesion and slenderness). The response values obtained for the two-way cohesion*friction term are

practically identical for all different parameter combinations and although clear higher response values are obtained for the two-way friction*slenderness and friction*live load interaction for the cases of slenderness equal to 0.25 and live load applied at voussoir 8 respectively, this wouldn't be enough to consider that this interaction terms had a significant effect on the response. Moreover, these visual assumptions are reinforced by the results obtained from the ANOVA analysis of the $\langle \alpha_c \rangle$ values obtained. It can be seen in Table 3 that not only the cohesion*friction two-way interaction term is not statistically significant, but the friction*slenderness and the friction*live load are as well considered as not statistically significant. Finally, in Figure 16 it can be seen that cohesion, slenderness and live load location parameters along with the cohesion*slenderness, slenderness*live load location and cohesion*live load location are the terms of the statistical model adopted which have a significant effect in the value of the collapse multiplier obtained for pointed arches under load scenario B.

The data independence and data normality assumptions were unfortunately not satisfied by the statistical model adopted. From the histogram presented in Figure 17, a certain degree of skewness is clearly observed. This observation, along with the presence of several outlier points in the standardized residual plots of Figure 17, reinforce the evidence observed regarding the non-linear relation between the parameters studied and the response of pointed arches under load scenario B and suggests that a parameter transformation (adoption of quadratic or exponential terms for the cohesion, slenderness and live load location terms) may be necessary in order to improve the quality of the statistical assessment of the results obtained for pointed arches under load scenario B.

5. Conclusions

The parametric analysis presented in this paper allowed to objectively identify the effect that slenderness, sharpness, friction ratio, cohesion and live load location parameters have in the collapse multiplier value and in the collapse mechanism of a masonry pointed arch using a non-standard limit analysis approach. The main findings drawn from this work are:

- Three different collapse mechanisms were observed for the studied pointed arched subjected to load scenario A: pure rotation, pure shearing and combined rotation-shearing mechanisms. On the other hand, only pure rotation and combined rotation-shearing mechanisms were obtained for the pointed arches subjected to load scenario B.

- Contrary to what has been previously pointed out by several authors, no statistically significant effect was found for the two-way sharpness*slenderness parameter on the response of pointed arches.

- The mechanical parameters studied play an important role in the value of collapse multipliers computed for the case of pointed arches subjected to load scenario A, whereas that only cohesion resulted to be statistically significant for the case of pointed arches subjected to load scenario B.

- Pointed arches can sustain larger concentrated loads if they are applied closer to the arch aunches than to its keystone.

6. Data availability statement

Some or all data, models, or code generated or used during the study are available in a repository or online in accordance with funder data retention policies [38, 38].

7. Acknowledgment

This work is supported by: Italian Ministry of University and Research PRIN 2017, project No. 2017HFPKZY (B88D19001130001); Sapienza Research Grants "Progetti Grandi" 2018 (B81G19000060005).

References

[1] A. Romano, Modelling, analysis and testing of masonry structures, Ph.D. thesis, Universita degli Studi di Napoli Federico II (7 2006). doi:10.6092/UNINA/

FEDOA/675.
URL http://www.fedoa.unina.it/id/eprint/675

[2] D. Aita, R. Barsotti, S. Bennati, Equilibrium of pointed, circular, and elliptical masonry arches bearing vertical walls, Journal of Structural Engineering (United States) 138 (7) (2012) 880–888. doi:10.1061/(ASCE)ST.1943-541X.0000522.

[3] N. Cavalagli, V. Gusella, L. Severini, The safety of masonry arches with uncertain geometry, Computers and Structures 188 (2017) 17–31. doi:10.1016/j.compstruc.2017.04.003.

[4] G. Brandonisio, M. Angelillo, A. De Luca, Seismic capacity of buttressed masonry arches, Engineering Structures 215 (2020). doi:10.1016/j.engstruct.2020.110661.

[5] G. Misseri, L. Rovero, Parametric investigation on the dynamic behaviour of masonry pointed arches, Archive of Applied Mechanics 87 (3) (2017) 385–404. doi:10.1007/s00419-016-1199-4.

[6] N. Cavalagli, V. Gusella, L. Severini, Lateral loads carrying capacity and minimum thickness of circular and pointed masonry arches, International Journal of Mechanical Sciences 115-116 (2016) 645–656. doi:10.1016/j.ijmecsci.2016.07.015.

[7] G. Misseri, M. DeJong, L. Rovero, Experimental and numerical investigation of the collapse of pointed masonry arches under quasi-static horizontal loading, Engineering Structures 173 (2018) 180–190. doi:10.1016/j.engstruct.2018.06.009.

[8] D. Aita, R. Barsotti, S. Bennati, Looking at the collapse modes of circular and pointed masonry arches through the lens of durand-claye's stability area method, Archive of Applied Mechanics 89 (8) (2019) 1537–1554. doi:10.1007/s00419-019-01526-z.

[9] D. Aita, R. Barsotti, S. Bennati, Arch-piers systems subjected to vertical loads: a comprehensive review of rotational, sliding and mixed collapse modes, Archive of Applied Mechanics 91 (1) (2021) 241–256. doi:10.1007/s00419-020-01766-4.

[10] S. Galassi, G. Misseri, L. Rovero, G. Tempesta, Analysis of masonry pointed arches on moving supports: A numeric predictive model and experimental evaluations, Lecture Notes in Mechanical Engineering (2020) 2048–2068Cited By 4; Conference of 24th Conference of the Italian Association of Theoretical and Applied Mechanics, AIMETA 2019 ; Conference Date: 15 September 2019 Through 19 September 2019; Conference Code:238859. doi:10.1007/978-3-030-41057-5_163.

[11] A. Romano, J. Ochsendorf, The mechanics of Gothic masonry arches, International Journal of Architectural Heritage 4 (1) (2010) 59–82. doi:10.1080/15583050902914660.

[12] C. Baggio, P. Trovalusci, Limit analysis for no-tension and frictional three-dimensional discrete systems, Mechanics of Structures and Machines 26 (3) (1998) 287–304. doi:10.1080/08905459708945496.

[13] C. Baggio, P. Trovalusci, Collapse behaviour of three-dimensional brick-block systems using non-linear programming, Structural Engineering and Mechanics 10 (2) (2000) 181–195. doi:10.12989/sem.2000.10.2.181.

[14] G. Milani, Simple lower bound limit analysis homogenization model for in- and out-of-plane loaded masonry walls, Construction and Building Materials 25 (12) (2011) 4426–4443. doi:10.1016/j.conbuildmat.2011.01.012.

[15] F. Portioli, C. Casapulla, M. Gilbert, L. Cascini, Limit analysis of 3d masonry block structures with non-associative frictional joints using cone programming, Computers and Structures 143 (2014) 108–121. doi:10.1016/j.compstruc.2014.07.010.

[16] G. Milani, A. Taliercio, Limit analysis of transversally loaded masonry walls using an innovative macroscopic strength criterion, International Journal of Solids and Structures 81 (2016) 274–293. doi:10.1016/j.ijsolstr.2015.12.004.

[17] M. Rossi, C. Calderini, B. Di Napoli, L. Cascini, F. Portioli, Structural analysis of masonry vaulted staircases through rigid block limit analysis, Structures 23 (2020) 180–190. doi:10.1016/j.istruc.2019.10.015.

[18] L. Cascini, R. Gagliardo, F. Portioli, LiABlock3D: A software Tool for Collapse Mechanism Analysis of Historic Masonry Structures, International Journal of Architectural Heritage 14 (1) (2020) 75–94. doi:10.1080/15583058.2018.1509155.

[19] N. Grillanda, A. Chiozzi, G. Milani, A. Tralli, Collapse behavior of masonry domes under seismic loads: An adaptive NURBS kinematic limit analysis approach, Engineering Structures 200 (2019). doi:10.1016/j.engstruct.2019.109517.

[20] R. Landolfo, R. Gagliardo, L. Cascini, F. Portioli, M. Malena, G. Tomaselli, G. de Felice, Rigid block and finite element analysis of settlement-induced failure mechanisms in historic masonry walls, Frattura ed Integrita Strutturale 14 (51) (2020) 517–533. doi:10.3221/IGF-ESIS.51.39.

[21] M. Pepe, M. Sangirardi, E. Reccia, M. Pingaro, P. Trovalusci, G. de Felice, Discrete and Continuous Approaches for the Failure Analysis of Masonry Structures Subjected to Settlements, Frontiers in Built Environment 6 (2020). doi:10.3389/fbuil.2020.00043.

[22] S. Tiberti, N. Grillanda, V. Mallardo, G. Milani, A Genetic Algorithm adaptive homogeneous approach for evaluating settlement-induced cracks in masonry walls, Engineering Structures 221 (2020). doi:10.1016/j.engstruct.2020.111073.

[23] M. Pepe, Numerical modeling for masonry: ALMA 2.0, A computational code for the limit analysis of historical masonry structures, Ph.D. thesis, Sapienza University of Rome (2 2020).

[24] M. Pepe, M. Pingaro, E. Reccia, P. Trovalusci, Micromodels for the in-plane failure analysis of masonry walls with friction: Limit analysis and dem-fem/dem approaches, Lecture Notes in Mechanical Engineering (2020) 1883–1895Conference of 24th Conference of the Italian Association of Theoretical and Applied Mechanics, AIMETA 2019 ; Conference Date: 15 September 2019 Through 19 September 2019; Conference Code:238859. doi:10.1007/978-3-030-41057-5_151.

[25] M. Pepe, M. Pingaro, P. Trovalusci, E. Reccia, L. Leonetti, Micromodels for the in-plane failure analysis of masonry walls: Limit analysis, FEM and FEM/DEM approaches, Frattura ed Integrita Strutturale 14 (51) (2020) 504–516. doi:10.3221/IGF-ESIS.51.38.

[26] M. Pepe, M. Pingaro, P. Trovalusci, Limit analysis approach for the in-plane collapse of masonry arches, Proceedings of the Institution of Civil Engineers - Engineering and Computational Mechanics (2021). doi:10.1680/jencm.20.00013.

[27] R. Livesley, Limit analysis of structures formed from rigid blocks, International Journal for Numerical Methods in Engineering 12 (12) (1978) 1853–1871. doi:10.1002/nme.1620121207.

[28] C. Baggio, P. Trovalusci, Discrete models for jointed block masonry walls, The Sixth North American Masonry Conference 2 (1993) 939–949.

[29] A. Rahman, T. Ueda, Experimental investigation and numerical modeling of peak shear stress of brick masonry mortar joint under compression, Journal of Materials in Civil Engineering 26 (9) (2014). doi:10.1061/(ASCE)MT.1943-5533.0000958.

[30] S. Jafari, J. Rots, R. Esposito, Core testing method to assess nonlinear shear-sliding behaviour of brick-mortar interfaces: A comparative experimental study, Construction and Building Materials 244 (2020). doi:10.1016/j.conbuildmat.2020.118236.

[31] D. Liberatore, N. Masini, L. Sorrentino, V. Racina, M. Sileo, O. AlShawa, L. Frezza, Static penetration test for historical masonry mortar, Construction and Building Materials 122 (2016) 810–822. doi:10.1016/j.conbuildmat.2016.07.097.

[32] L. Bejarano-Urrego, E. Verstrynge, G. Giardina, K. Van Balen, Crack growth in masonry: Numerical analysis and sensitivity study for discrete and smeared crack modelling, Engineering Structures 165 (2018) 471–485. doi:10.1016/j.engstruct.2018.03.030.

[33] J. Milosevic, A. Gago, M. Lopes, R. Bento, Experimental assessment of shear strength parameters on rubble stone masonry specimens, Construction and Building Materials 47 (2013) 1372–1380. doi:10.1016/j.conbuildmat.2013.06.036.

[34] A. Rafiee, M. Vinches, Mechanical behaviour of a stone masonry bridge assessed using an implicit discrete element method, Engineering Structures 48 (2013) 739–749. doi:10.1016/j.engstruct.2012.11.035.

[35] F. Masi, I. Stefanou, V. Maffi-Berthier, P. Vannucci, A Discrete Element Method based-approach for arched masonry structures under blast loads, Engineering Structures 216 (2020). doi:10.1016/j.engstruct.2020.110721.

[36] D. Weed, A. Tennant, M. Motamedi, K. Gourav, C. Foster, B. Reddy, Finite element model application to flexural behavior of cement stabilized soil block masonry, Materials and Structures/Materiaux et Constructions 53 (3) (2020). doi:10.1617/s11527-020-01490-z.

[37] S. Zhang, K. Beyer, Numerical investigation of the role of masonry typology on

shear strength, Engineering Structures 192 (2019) 86–102. doi:10.1016/j.engstruct.2019.04.026.

[38] A. Jiménez Rios, M. Pingaro, E. Reccia, B. Nela, P. Trovalusci, Data from the parametric analysis of masonry pointed arches with limit analysis subjected to vertical self-weight plus a proportional horizontal live load (Jul. 2021). doi:10.5281/zenodo.5146824.
URL https://doi.org/10.5281/zenodo.5146824

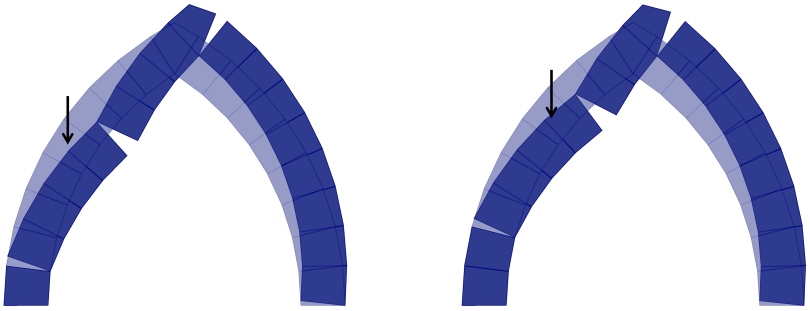

(a) Live load applied to block 8, $\alpha_c = 32.25203$.

(b) Live load applied to block 10, $\alpha_c = 19.74183$.

(c) Live load applied to block 12, $\alpha_c = 13.30609$.

(d) Live load applied to block 14, $\alpha_c = 9.20905$.

Figure 9: Effect of the live load location parameter on the collapse mechanisms under load scenario B.

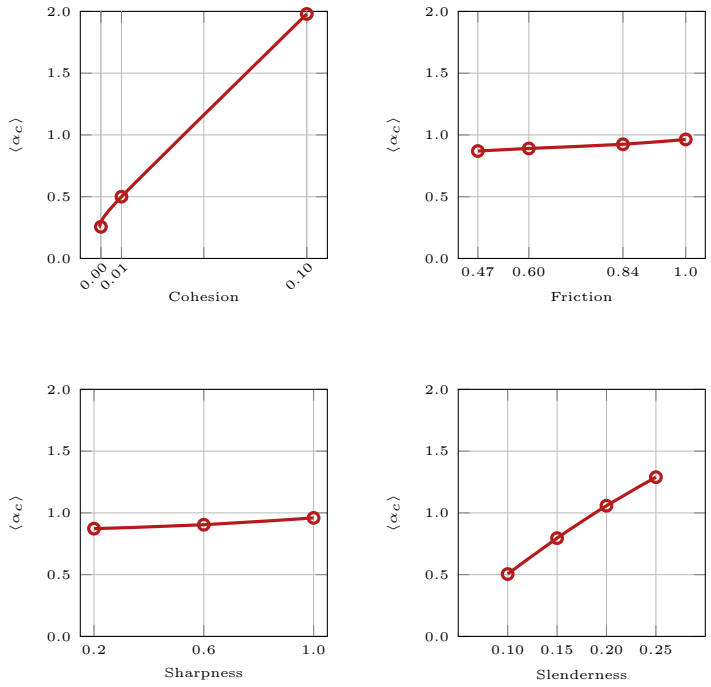

Figure 10: Main effect plots for load scenario A.

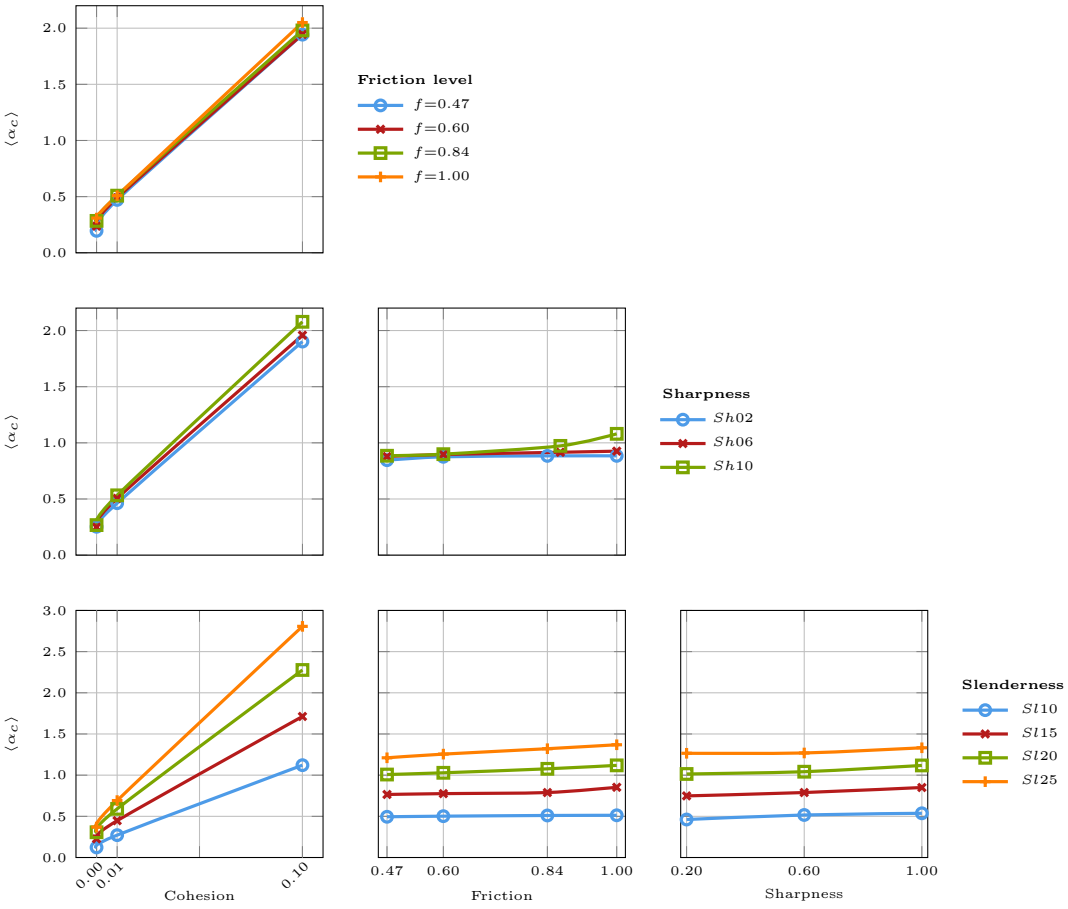

Figure 11: Interaction effect plots for load scenario A.

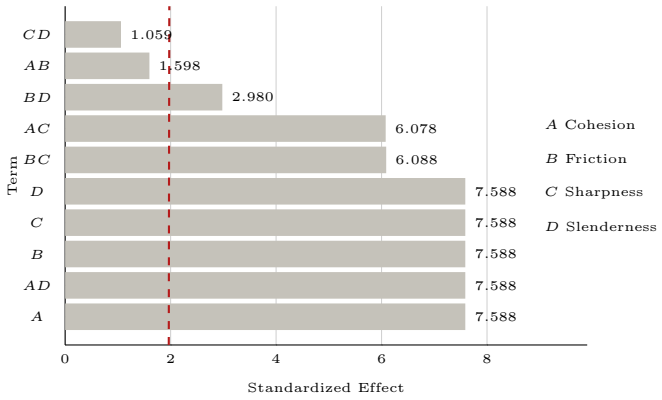

Figure 12: Pareto chart of the standardized effects: magnitude and importance of the different main factors and factor interactions effects for load scenario A.

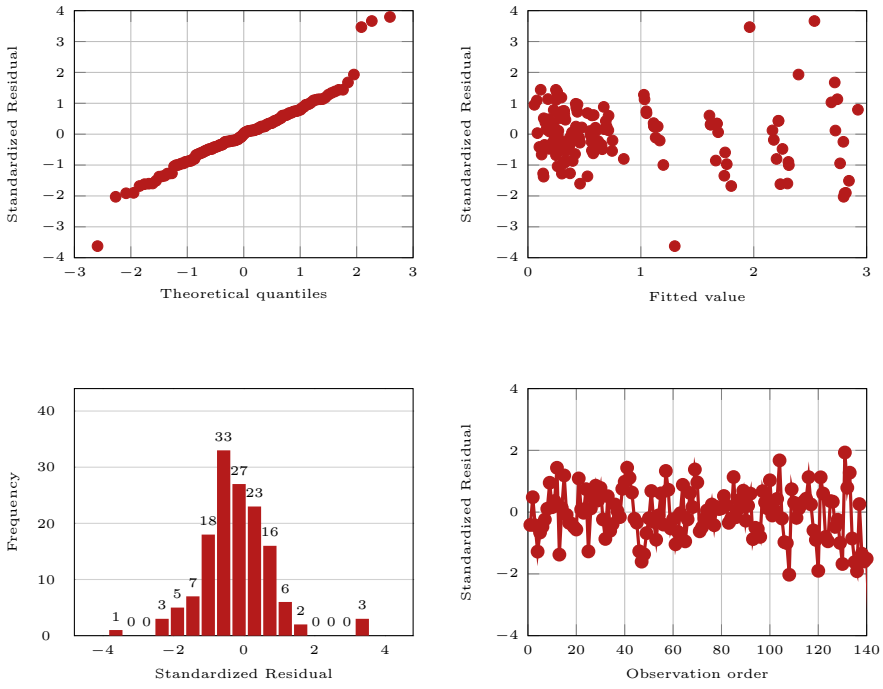

Figure 13: Normal probability, histogram and standardized residual plots for the pointed arches under load scenario A.

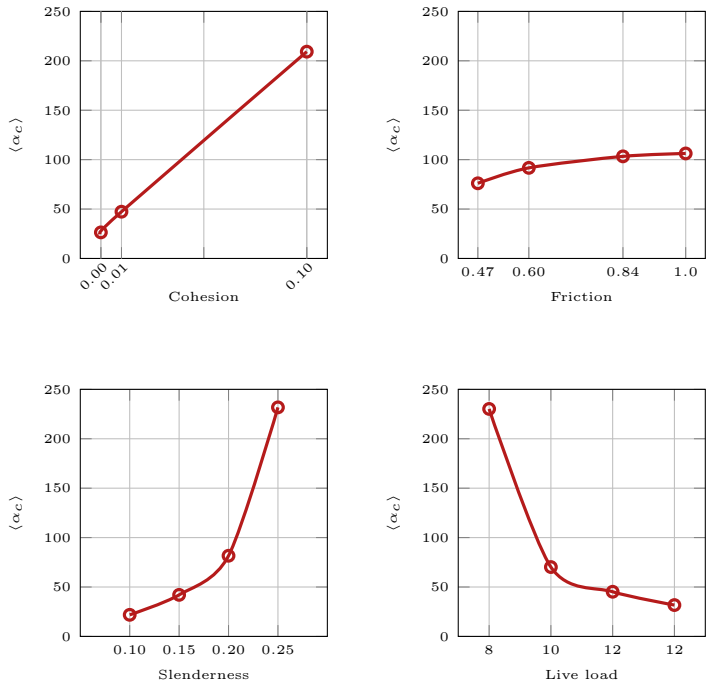

Figure 14: Main effect plots for load scenario B.

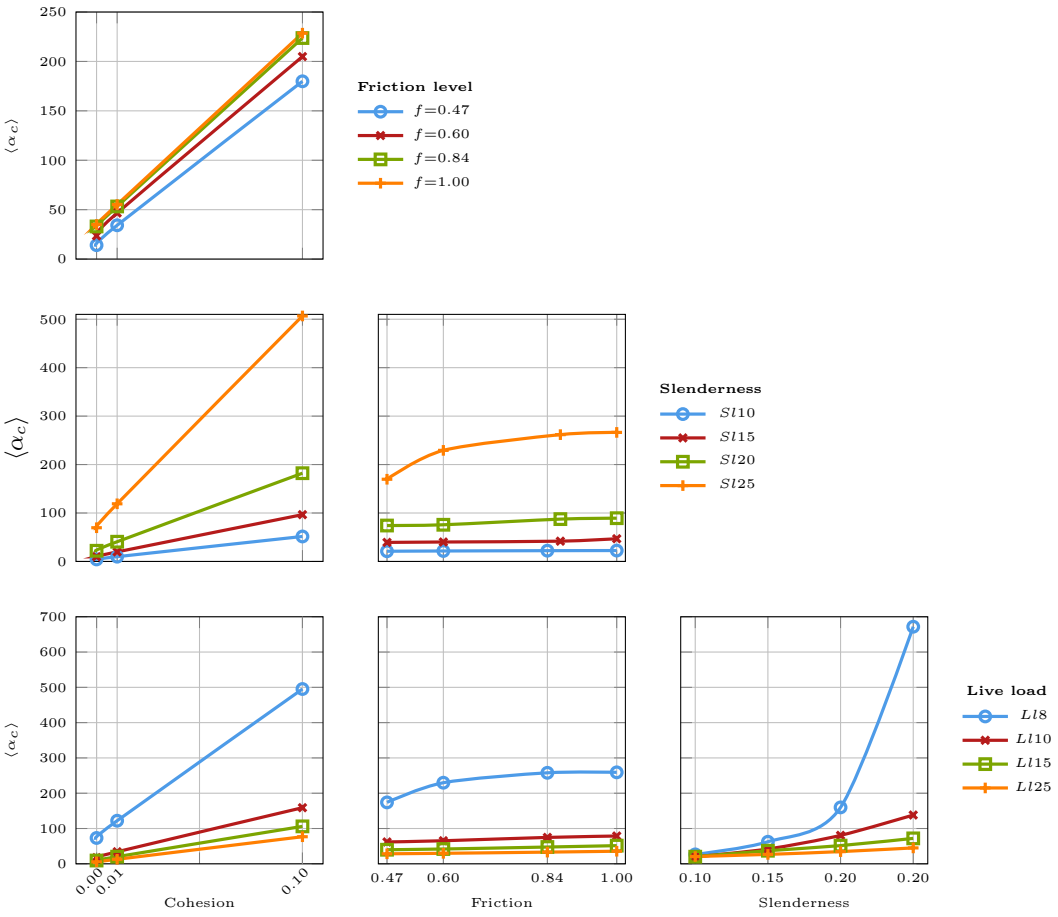

Figure 15: Interaction effect plots for load scenario B.

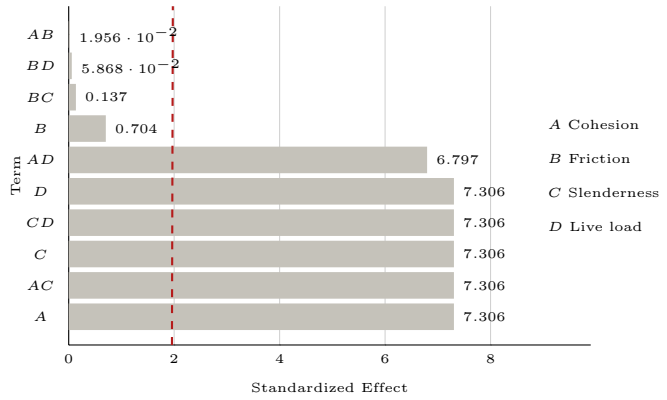

Figure 16: Pareto chart of the standardized effects: magnitude and importance of the different main factors and factor interactions effects for load scenario B.

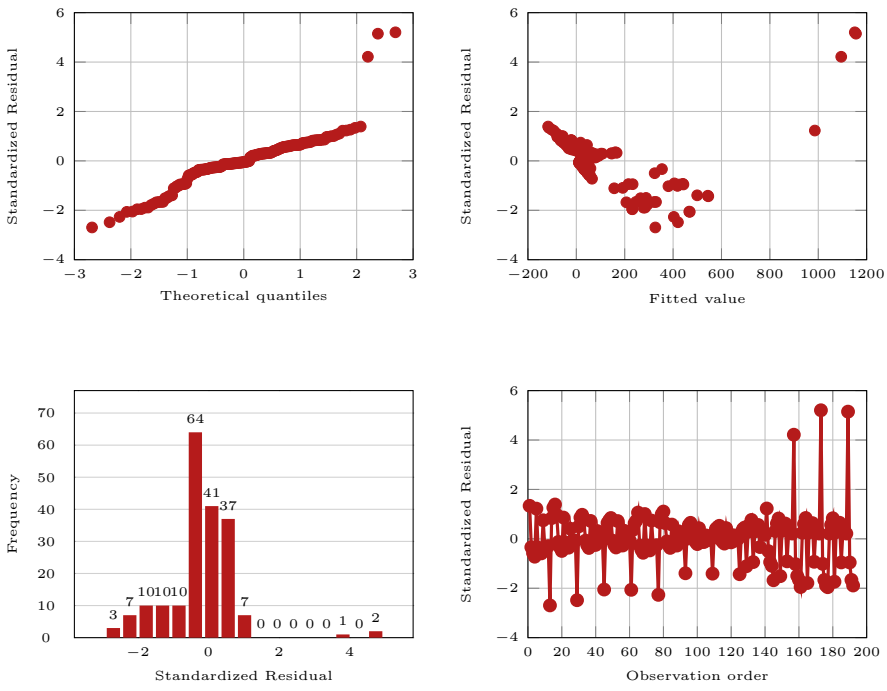

Figure 17: Normal probability, histogram and standardized residual plots for the pointed arches under load scenario B.